Chemical Science

ROYAL SOCIETY OF CHEMISTRY

EDGE ARTICLE

View Article Online
View Journal | View Issue

Cite this: *Chem. Sci.*, 2025, **16**, 18161

All publication charges for this article have been paid for by the Royal Society of Chemistry

Received 23rd June 2025
Accepted 2nd September 2025

DOI: 10.1039/d5sc04618a

rsc.li/chemical-science

Spatial functionality gradient in a ZIF-8 thin film membrane

KM. Archana Yadav, Girish Mishra, † Susmita Kundu,† Soumya Ghosh and Ritesh Haldar *

Zeolitic imidazolate framework-8 (ZIF-8), constructed from Zn^{2+} ions and 2-methylimidazole (mIm) linkers, is widely recognized for its excellent thermal and chemical stability, making it a strong candidate for chemical separation and heterogeneous catalysis. In this study, we report a new crystalline phase of functionalized ZIF-8 featuring a spatially graded distribution of chemical functionalities. This anisotropic functionalization is achieved *via* a vapor-phase process applied to a ZIF-8 monolithic film. Anisotropic diffusion of a reactive linker—imidazole-2-carboxaldehyde (CHO-Im)—into the ZIF-8 monolith results in a gradient incorporation of CHO-Im, yielding a ZIF-8–CHO monolith. Spatial anisotropy of the CHO functional groups is confirmed through X-ray diffraction, scanning electron microscopy, and vibrational spectroscopy. To demonstrate its potential, we fabricated an anodic aluminium oxide-supported membrane and highlighted its enhanced gas permselectivity compared to pristine membranes.

Introduction

Porous materials with tunable pore structures and chemical functionalities are highly sought after for the development of advanced chemical separation technologies (membranes). Among the contemporary materials, metal–organic frameworks (MOFs) stand out due to their exceptional chemical modularity, enabling the tailored design of materials for specific applications. Some of the MOFs (zeolitic imidazolate frameworks, Zr-based MOFs and others) have been extensively investigated for gas storage, molecular separation, catalysis, selective ion conduction, and beyond. Over the past two decades, a vast array of MOF structures with diverse and specialized chemical characteristics have been discovered. A notable advancement in this field is the development of mixed-component or multivariate materials that incorporate multiple organic linkers or metal nodes in controlled ratios to generate synergistic and emergent properties (enhanced selectivity,[2] adsorption,[3,4] diffusion,[5,6] excitation energy transfer,[7–9] electron–hole separation,[10] and catalysis[11]). While these mixed-component systems have shown considerable promise in enhancing adsorption selectivity[12] (CO_2 under humid conditions,[2] CH_4 adsorption,[3] and H_2 adsorption[4]), precise spatial control over the distribution of chemical functionalities remains a significant challenge.[4,13,14] In polycrystalline MOF powders, mixed-linker strategies are relatively well-established[14] (for example, spatial distribution modulation in core–shell type crystals);[15] however, translating this approach to device-relevant architectures such as thin films presents even greater technical hurdles.

Zeolitic imidazolate frameworks (ZIFs),[16–18] a prominent subclass of MOFs, have been extensively investigated for their potential in chemical separations,[17] owing to their excellent chemical stability and functional versatility.[16] The incorporation of multiple linkers in ZIFs—through mixed-linker strategies—has been particularly successful, enabling fine-tuning of their properties.[19–21] Moreover, ZIFs have been fabricated into thin-film membranes, and functional heterostructures composed of ZIFs have been realized. Prior studies have consistently demonstrated that such heterostructures yield enhanced performance, which has been attributed to the presence of chemically distinct interfaces (*e.g.*, in core–shell architectures and bilayer films) and the cooperative behaviour of multiple linkers in mixed-linker systems. In the present study, we move beyond the traditional strategies of creating discrete interfaces or uniformly mixing chemical functionalities. We demonstrate that spatially gradient chemical functionality within ZIFs, specifically within the ZIF-8 structure, is feasible and this feature can tailor the molecular sieving properties. Scheme 1 illustrates a spatial functional gradient in a MOF monolith, in contrast to the conventional mixed-linker and MOF-on-MOF heterostructure. In this study, we applied the concept of a spatial chemical functionality gradient to a monolithic film of ZIF-8, constructed by linking Zn^{2+} and 2-methylimidazole (mIm). Specifically, a –CHO functionalized imidazole linker (CHO-Im) was gradiently distributed within the ZIF-8 monolith using a vapor-phase linker exchange reaction.

Our investigation aimed to demonstrate the feasibility of creating such a chemical functionality gradient within the thin

Tata Institute of Fundamental Research Hyderabad, Gopanpally, 500046 Hyderabad, India. E-mail: riteshhaldar@tifrh.res.in

† These authors contributed equally.

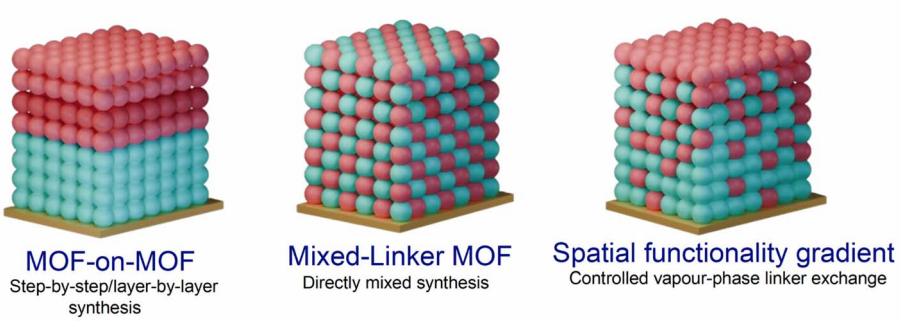

Scheme 1 A schematic illustration of mixed-linker MOF structures with different possible spatial configurations and fabrication methods; left to right: MOF-on-MOF, homogeneously mixed-linker and the spatial gradient, which is demonstrated in the current work. Two differently colored spheres are used to represent different linker's presence in the MOF.

film of ZIF-8. The results revealed the formation of a unique mixed-linker ZIF-8 monolith, but not a ZIF-8_ZIF-90 mixed crystalline phase film (ZIF-90 is made of Zn^{2+} and CHO-Im). In the monolith structure, CHO-Im was distributed according to a diffusion gradient leveraged by the vapor-phase reaction. This spatial distribution gradient significantly enhanced the molecular sieving properties of the material. Here, we detail the principle and methodology used to achieve this spatial gradient functionality in ZIF-8 and reveal its distinctive properties.

Results and discussion

Vapour-phase ZIF-8 functionalization

ZIF-8 exhibits a sodalite topology characterized by distinct hexagonal pore windows approximately 3.4 Å in diameter.[1] While the Zn^{2+}–N coordination bonds in ZIF-8 are chemically stable, their reversible nature permits linker-exchange reactions. As a result, the 2-methylimidazole (mIm) linkers in ZIF-8 can be partially or fully replaced with other substituted imidazoles, enabling the synthesis of new ZIFs or mixed-linker variants. This exchange can be achieved through solvent-assisted methods or vapor-phase reactions, as demonstrated in previous studies.[22–26] An alternative approach involves the direct incorporation of additional imidazole-based linkers alongside mIm during synthesis to produce mixed-linker ZIFs. It is important to note that such linker mixing strategies have been predominantly explored in polycrystalline powder ZIF-8, often yielding structurally distinct ZIF phases.[22,27,28] In powder ZIFs, the isotropic diffusion of linkers into the particles facilitates the formation of new ZIF structures, as reported in earlier literature.[29–31] In some cases, slow linker diffusion can lead to the development of core–shell-type heterostructures.[32–34] Another theoretically possible outcome is a gradient distribution of the exchange linker; however, such configurations have not been reported. This absence is likely due to the broad distribution of crystallite sizes in powders, which results in variable diffusion rates and renders the identification of a gradient phase challenging. Moreover, the functional impact of such a gradient distribution is difficult to evaluate in powder samples of ZIFs or other MOFs. In the present study, we aim to investigate the feasibility and functional implications of gradient linker distributions within ZIF-8 structures.

In this study, we employed a vapor-phase linker exchange strategy on ZIF-8 monolithic thin films to investigate the feasibility of achieving gradient functional conversion, as depicted in Scheme 1. The choice of a monolithic thin film was intentional, as it facilitates anisotropic linker diffusion along the film's thickness, thereby providing a suitable platform to explore spatial variations in composition. Under conditions of uniform and efficient linker exchange, a complete transformation from ZIF-8 to ZIF-90 would be anticipated using 2-carboxaldehyde imidazole (CHO-Im) as the exchange linker. However, other outcomes are also possible, such as the formation of a homogeneous ZIF-8_ZIF-90 mixture or a spatially graded composite of the two (Fig. S1). In the sections that follow, we detail the synthesis methodology and provide evidence that the vapor-phase exchange results in a spatial gradient of CHO-Im incorporation. Rather than yielding a simple mixture or full conversion, the process gives rise to a CHO-Im functionalized ZIF-8 structure—hereafter referred to as ZIF-8–CHO (Fig. 1a). We further demonstrate that this spatially graded monolith exhibits enhanced molecular sieving performance, underscoring the significance of gradient linker distribution in tuning material properties.

We have first synthesized a ZIF-8 monolithic film on –OH functionalized Au substrates using a previously established solution phase layer-by-layer methodology[35] (see the SI for experimental details). The grown thin film exhibited sharp diffraction peaks corresponding to phase-pure ZIF-8 (Fig. 1b). To introduce a new linker in this ZIF-8 film, we have adopted a vapour-phase linker exchange reaction. First, the ZIF-8 film was activated and then placed in a closed glass chamber loaded with CHO-Im for 72 h at 353 K. After cooling down to room temperature, the modified film was washed thoroughly using dichloromethane and dried under vacuum at 323 K for 12 h. The purpose of thorough cleaning was to ensure the removal of unreacted and trapped linkers. The treated film was then examined by XRD, infrared reflection absorption spectroscopy and SEM (Fig. 1b–e). The vapour phase treatment can give rise four possible structures: (I) fully converted ZIF-90, (II) ZIF-8/ZIF-90 mixed phases, (III) ZIF-8_ZIF-90 bilayer structure and (IV)

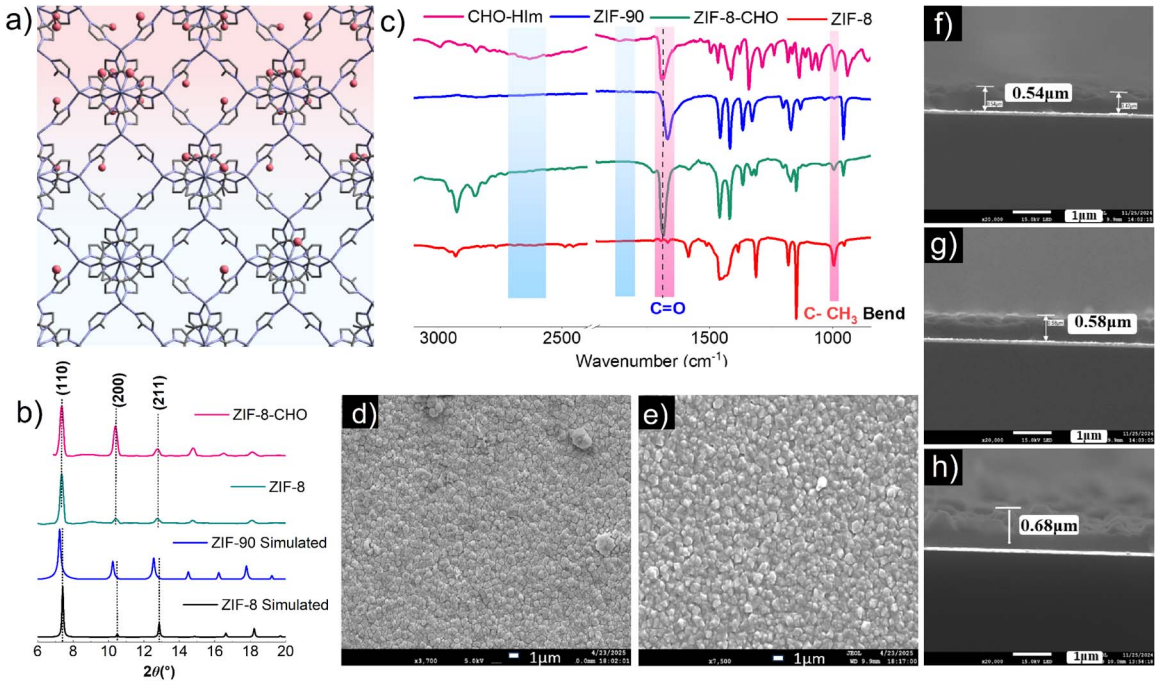

Fig. 1 (a) Illustration of the ZIF-8–CHO heterostructure thin film (red sphere = CHO group). (b) Out-of-plane XRD patterns of ZIF-8–CHO and ZIF-8 with simulated ZIF-8 and ZIF-90. (c) IRRAS of ZIF-8–CHO, ZIF-8, ZIF-90(powder), and 2-imidazolecarboxaldehyde (powder). (d and e) SEM morphology of ZIF-8 and ZIF-8–CHO. (f–h) Cross-section SEM images of ZIF-8, ZIF-8–CHO, and ZIF-8_ZIF-90, respectively.

spatial gradient of CHO-Im functionalization in ZIF-8. Cases II-IV are illustrated in Fig. S1. The main difference between II and IV is the distribution of CHO-Im linkers. Case iii may arise, if the top ZIF-90 layer acts as a barrier to CHO-Im diffusion. The XRD pattern of the 72 h modified film (ZIF-8–CHO) exhibited a very similar pattern to that of parent ZIF-8 (Fig. 1b). Note, a time dependent study confirmed that 72 h was needed for the conversion (see Fig. S2). These XRD data confirmed that the lattice dimension did not change by the vapour-phase reaction. However, the intensity ratio of the peaks corresponding to (110) and (200) planes changed substantially after the vapour phase reaction. Note that ZIF-8 and ZIF-90 unit cell dimensions differ by a small amount, and the crystal symmetry is the same. An earlier investigation of mixed-linker ZIF indicated that the unit cell dimensions do not differ in the mixed-phase.[19] Hence, we assumed that ZIF-90 conversion is possibly successful.

To confirm the presence of CHO-Im, we have carried out IRRAS experiments (Fig. 1c). The ZIF-8–CHO film exhibited a strong absorption at 1685 cm^{-1} corresponding to C=O stretching vibration. This feature was missing in the parent ZIF-8 structure. A few additional features are: (i) the C–CH_3 bending mode at 995 cm^{-1} is present in ZIF-8–CHO, confirming the presence of ZIF-8, (ii) the absence of free –NH modes (1848, 1820, and 2400–3200 cm^{-1}) in ZIF-8–CHO confirmed that unreacted CHO-Im is absent, and (iii) C=O stretching frequency in ZIF-8–CHO at 1685 cm^{-1} is different than that in neat ZIF-90 (1670 cm^{-1}). The above observations rule out the possibility of a case i type structure. The most striking revelation was the unique C=O stretching mode. In the absence of non-coordinated CHO-Im, we can attribute the shift in C=O mode to lattice constraints (*vide infra*). Note that the observed C=O stretching did not arise because of incomplete reaction, as can be seen from reaction time-dependent IRRAS (Fig. S2). On a shorter time scale, C=O stretching at 1685 cm^{-1} is very weak and the intensity is enhanced for a longer time of exchange reaction (1683 cm^{-1}).

Fig. 1d and e clearly indicate that the ZIF-8 and ZIF-8–CHO thin films are homogeneous and continuously grown, thus avoiding the formation of island type structures. This homogeneity is more evident in Fig. 1f and g, which show the cross-section SEM view. Vapour-phase conversion did not change the film thickness. In contrast, a solvothermal growth of ZIF-90 on top of ZIF-8 did change the film thickness (Fig. 1h, the synthesis of bilayer ZIF-8_ZIF-90 is discussed in the SI).

To confirm that the unique C=O stretching frequency is indeed due to lattice constraints, we have calculated (density functional theory) and compared the C=O vibration of neat ZIF-90 and a 50% doped CHO-Im in ZIF-8 lattice (see computational details in the SI). As shown in Fig. 2, it is evident that the C=O vibration frequencies are shifted to a higher wavenumber, as observed in the experiment.

Next, X-ray photoelectron spectroscopy (XPS) was performed to evaluate the chemical conversion of the ZIF-8 thin film (Fig. 3). Note that the XPS data mostly provide information about the top ~10 nm of the thin film. The Zn $2p_{3/2}$ core-level spectra exhibited a gradual increase in binding energy from 1022.0139 eV in pristine ZIF-8 to 1022.023 eV in ZIF-8–CHO. This binding energy increment indicates modifications in the local coordination environment of zinc, likely due to the introduction of electron-withdrawing aldehyde functionalities.

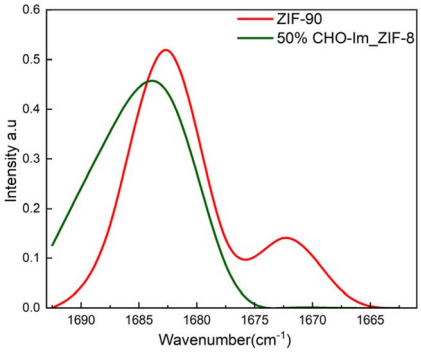

Fig. 2 DFT calculated IR frequency plots of ZIF-90 and 50% CHO-Im in ZIF-8.

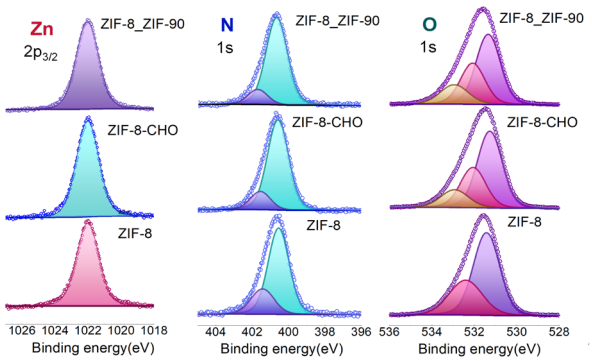

Fig. 3 The XPS spectra of ZIF-8, ZIF-8–CHO and ZIF-8_ZIF-90 for Zn, N, and O.

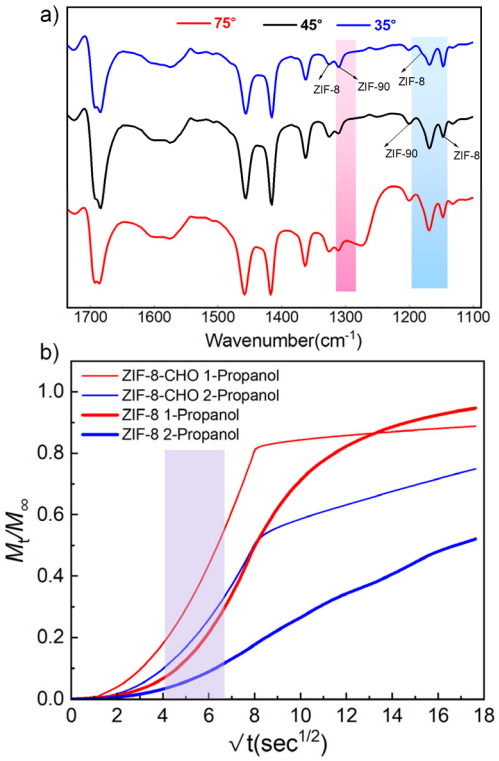

Fig. 4 (a) Angle dependent IRRAS of ZIF-8–CHO at 35°, 45° and 75°, and (b) 1-propanol and 2-propanol vapour uptake profiles for the ZIF-8 and ZIF-8–CHO thin films. The shaded region was used for slope calculation.

The N 1s spectra revealed two components corresponding to N–H and N–Zn bonding. In ZIF-8, these peaks were observed at 401.435 eV and 400.549 eV, respectively. In ZIF-8–CHO, the binding energies shifted to 401.5583 eV (N–H) and 400.5845 eV (N–Zn), attributed to the electronic effects of the CHO substituents. The O 1s spectra also showed significant changes consistent with functional group variation. For ZIF-8, the Zn–O and O–H components appeared at 532.416 eV and 531.435 eV, respectively. Upon functionalization to ZIF-8–CHO, the O 1s spectrum showed three components: Zn–O at 532.0860 eV, OH/MeOH at 531.2939 eV, and a C=O peak at 532.9602 eV, indicating the successful incorporation of aldehyde functionalities (~41% CHO-Im). Note that the comparison of Zn, N and O binding energies for ZIF-8–CHO and bilayer ZIF-8_ZIF-90 shows clear difference, confirming that the nature of functionalization is very different.

Spatial distribution of the functionalized linker

To gain further insight into the incorporation of the 2-imidazolecarboxaldehyde (CHO-HIm) linker within the ZIF-8 framework, angle-dependent IRRAS was performed (Fig. 4a).[36] Spectra were collected at three incident angles 35°, 45° and 75°. Analysis of the spectra revealed that the intensity of the peaks at 1325 cm^{-1} (H–CO stretching), 1200 cm^{-1} (C–N stretching), and 1168 cm^{-1}, characteristic[19] of ZIF-90, increases progressively from 35° to 75°. In contrast, the peaks at 1310 cm^{-1} and 1146 cm^{-1}, associated with ZIF-8,[37] show a decreasing trend of intensity. This angle-dependent spectral behaviour indicates a compositional gradient within the film, with the CHO-Im linker predominantly incorporated near the surface. We attribute this spatial distribution to the linker vapour diffusion along the film thickness.

To confirm that the functionalization of ZIF-8 with the CHO-Im linker was successful, we performed 1 and 2-propanol vapour uptake measurements on neat ZIF-8 and ZIF-8–CHO thin films. To do so, both thin films were grown on Au-coated quartz crystal sensors (see the Experimental section) and the fundamental frequencies were measured under a constant flow of saturated vapours of 1 and 2-propanol.[6,38,39] The uptake profiles are shown in Fig. 4b. Comparison of the slopes (in the linear region of the uptake profiles) confirmed that the functionalization of ZIF-8 by CHO-Im reduces the 1-propanol/2-propanol selectivity. This is according to the literature precedence.[40,41] Addition of the CHO-group reduces the isomer recognition, thereby decreasing the diffusion selectivity.

CO_2/N_2 permselectivity

To investigate the influence of the spatial gradient on molecular sieving performance, we fabricated ZIF-8–CHO and ZIF-8_ZIF-90 membranes on porous anodic alumina oxide (AAO; pore size ~ 100 nm) and compared the CO_2/N_2 permselectivity

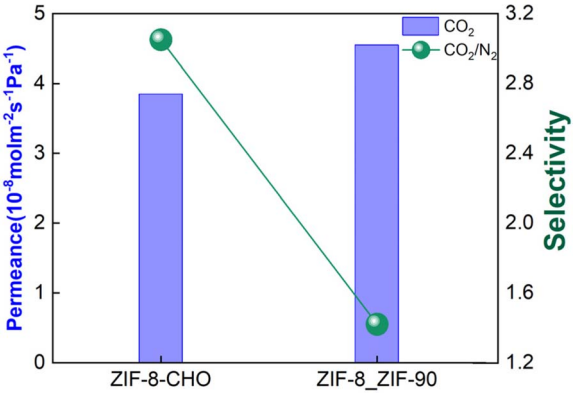

Fig. 5 CO_2 permeance and CO_2/N_2 selectivity of ZIF-8–CHO and ZIF-8_ZIF-90 (CO_2 gas permeance = purple bar, CO_2/N_2 selectivity = green circle).

(Fig. 4). The synthesis methodologies were similar to those used for film growth on Au substrates. The continuous film formation was tested by SEM experiments (Fig. S3 and S4). The gas permeation experiments were carried out using a custom made Wicke–Kallenbach setup (Fig. S5) at 303 K under a constant transmembrane pressure (4 bar). We have also performed pressure dependent permeance measurements on both of the membranes and realized similar permeance values, confirming the absence of any pinhole (Fig. S6). An earlier study reported that a neat ZIF-8 membrane, fabricated using a similar methodology to that in the current work, exhibited an ideal CO_2/N_2 permselectivity of 2.2 (CO_2 permeance $\sim$ 9.5 ($\pm$2) $\times$ 10^{-8} mol m^{-2} s^{-1} Pa^{-1}).[42] We observed that in the case of ZIF-8–CHO, the ideal CO_2/N_2 permselectivity was $\sim$3 (CO_2 permeance $\sim$ 3.8 ($\pm$2) $\times$ 10^{-8} mol m^{-2} s^{-1} Pa^{-1}) (Fig. 5). The enhanced selectivity is attributed to the inclusion of –CHO functionality in the ZIF-8 lattice, leading to a constricted pore window and specific CO_2–C=O (CHO) interaction. Interestingly, the ZIF-8_ZIF-90 membrane exhibited a much lower permselectivity of 1.4 (Fig. 4). Hence, it is evident that the presence of only ZIF-90 does not enhance the selectivity; rather, the spatial functional gradient in ZIF-8–CHO does enhance the sieving performance. Note that a homogeneously mixed ZIF-8–CHO membrane synthesis was not possible and hence a direct comparison could not be done.

Conclusions

Functional porous solids, like ZIFs, are significant materials for chemical separation. Designing the pore surface of ZIFs with multiple chemical functionalities is advantageous in the context of selective adsorption. However, controlling the spatial distribution of chemical functionalities is rarely achieved. Leveraging the vapour phase linker exchange reaction and the diffusion gradient, a spatially gradient functionalized ZIF-8 thin film is realized. We demonstrate that the vapor phase reaction yields a functionalized ZIF-8 lattice, and the unique pore environment shows improved gas permselectivity, compared to the pristine MOFs. The findings presented here demonstrate a potential strategy to alter and tune porous thin membranes for advanced separation technology. Also, the impact of graded spatial distribution needs further study to explore its full potential for chemical separation.

Author contributions

KM. A. Y. and R. H. conceived the idea and planned the experiments, A. Y. performed the experiments and characterization, S. K. helped with SEM, G. M. performed the DFT calculations with the guidance of S. G., and S. K. and G. M. contributed equally. The manuscript draft was prepared with the inputs from all authors.

Conflicts of interest

There are no conflicts to declare.

Data availability

All the data are available upon request to the corresponding author.

Supplementary information is available. See DOI: **https://doi.org/10.1039/d5sc04618a**.

Acknowledgements

We acknowledge the financial support from Science and Engineering Research Board (SERB), Govt. of India (project no.: SRG/2022/000927) and intramural funds at TIFR Hyderabad from the Department of Atomic Energy (DAE), India, under project identification number RTI 4007.

References

1 K. S. Park, Z. Ni, A. P. Côté, J. Y. Choi, R. Huang, F. J. Uribe-Romo, H. K. Chae, M. O'Keeffe and O. M. Yaghi, *Proc. Natl. Acad. Sci. U. S. A.*, 2006, **103**, 10186–10191.
2 N. T. T. Nguyen, H. Furukawa, F. Gándara, H. T. Nguyen, K. E. Cordova and O. M. Yaghi, *Angew. Chem., Int. Ed.*, 2014, **53**, 10645–10648.
3 B. Li, H.-M. Wen, H. Wang, H. Wu, T. Yildirim, W. Zhou and B. Chen, *Energy Environ. Sci.*, 2015, **8**, 2504–2511.
4 H. Deng, C. J. Doonan, H. Furukawa, R. B. Ferreira, J. Towne, C. B. Knobler, B. Wang and O. M. Yaghi, *Science*, 2010, **327**, 846–850.
5 S. Zhou, O. Shekhah, A. Ramírez, P. Lyu, E. Abou-Hamad, J. Jia, J. Li, P. M. Bhatt, Z. Huang, H. Jiang, T. Jin, G. Maurin, J. Gascon and M. Eddaoudi, *Nature*, 2022, **606**, 706–712.
6 T. Maity, S. Sarkar, S. Kundu, S. Panda, A. Sarkar, R. Hammad, K. Mandal, S. Ghosh, J. Mondal and R. Haldar, *Nat. Commun.*, 2024, **15**, 9636.
7 J. Jia, L. Gutiérrez-Arzaluz, O. Shekhah, N. Alsadun, J. Czaban-Jóźwiak, S. Zhou, O. M. Bakr, O. F. Mohammed and M. Eddaoudi, *J. Am. Chem. Soc.*, 2020, **142**, 8580–8584.

8 R. Haldar, M. Jakoby, A. Mazel, Q. Zhang, A. Welle, T. Mohamed, P. Krolla, W. Wenzel, S. Diring, F. Odobel, B. S. Richards, I. A. Howard and C. Wöll, *Nat. Commun.*, 2018, **9**, 4332.
9 M. Oldenburg, A. Turshatov, D. Busko, S. Wollgarten, M. Adams, N. Baroni, A. Welle, E. Redel, C. Wöll, B. S. Richards and I. A. Howard, *Adv. Mater.*, 2016, **28**, 8477–8482.
10 Z. Xu, A. Chandresh, A. Mauri, M. Esmaeilpour, V. Monnier, F. Odobel, L. Heinke, W. Wenzel, M. Kozlowska, S. Diring, R. Haldar and C. Wöll, *Angew. Chem., Int. Ed.*, 2024, **63**, e202414526.
11 Y. Yin, S. Feng, X. Xu, Y. Liu, Y. Li, L. Gao, X. Zhou, J. Dong, Y. Wu, J. Su, J.-L. Zuo, S. Yuan and J. Zhu, *J. Am. Chem. Soc.*, 2025, **147**, 16481–16493.
12 M. Mon, R. Bruno, E. Tiburcio, M. Viciano-Chumillas, L. H. G. Kalinke, J. Ferrando-Soria, D. Armentano and E. Pardo, *J. Am. Chem. Soc.*, 2019, **141**, 13601–13609.
13 K. Roztocki, M. K. Dudek, M. Szufla, F. Formalik, V. Bon, A. Krawczuk, P. Paluch, S. Kaskel and D. Matoga, *Chem. Mater.*, 2024, **36**, 8578–8587.
14 X. Kong, H. Deng, F. Yan, J. Kim, J. A. Swisher, B. Smit, O. M. Yaghi and J. A. Reimer, *Science*, 2013, **341**, 882–885.
15 S. Jeong, J. Seong, S. W. Moon, J. Lim, S. B. Baek, S. K. Min and M. S. Lah, *Nat. Commun.*, 2022, **13**, 1027.
16 Z. Zheng, Z. Rong, H. L. Nguyen and O. M. Yaghi, *Inorg. Chem.*, 2023, **62**, 20861–20873.
17 A. Phan, C. J. Doonan, F. J. Uribe-Romo, C. B. Knobler, M. O'Keeffe and O. M. Yaghi, *Acc. Chem. Res.*, 2010, **43**, 58–67.
18 R. Banerjee, A. Phan, B. Wang, C. Knobler, H. Furukawa, M. O'Keeffe and O. M. Yaghi, *Science*, 2008, **319**, 939–943.
19 K. Eum, K. C. Jayachandrababu, F. Rashidi, K. Zhang, J. Leisen, S. Graham, R. P. Lively, R. R. Chance, D. S. Sholl, C. W. Jones and S. Nair, *J. Am. Chem. Soc.*, 2015, **137**, 4191–4197.
20 J. A. Thompson, C. R. Blad, N. A. Brunelli, M. E. Lydon, R. P. Lively, C. W. Jones and S. Nair, *Chem. Mater.*, 2012, **24**, 1930–1936.
21 J. A. Thompson, N. A. Brunelli, R. P. Lively, J. R. Johnson, C. W. Jones and S. Nair, *J. Phys. Chem. C*, 2013, **117**, 8198–8207.
22 Q. T. Nguyen, J. Y. Lee, Y. Bae, Y.-R. Lee, Y. Song, S. H. Kim, K.-Y. Baek and J. Na, *ChemSusChem*, 2025, **18**, e202401968.
23 W. Wu, J. Su, M. Jia, Z. Li, G. Liu and W. Li, *Sci. Adv.*, 2020, **6**, eaax7270.
24 P. Su, M. Tu, R. Ameloot and W. Li, *Acc. Chem. Res.*, 2022, **55**, 186–196.
25 L. Xue, G. Luo, X.-c. Yang, Y. Qin and B. Zhang, *Innovation Mater.*, 2024, **2**, 100047.
26 J. Marreiros, L. Van Dommelen, G. Fleury, R. de Oliveira-Silva, T. Stassin, P. Iacomi, S. Furukawa, D. Sakellariou, P. L. Llewellyn, M. Roeffaers and R. Ameloot, *Angew. Chem., Int. Ed.*, 2019, **58**, 18471–18475.
27 Q. Hou, Y. Wu, S. Zhou, Y. Wei, J. Caro and H. Wang, *Angew. Chem., Int. Ed.*, 2019, **58**, 327–331.
28 S. Berens, F. Hillman, H.-K. Jeong and S. Vasenkov, *Microporous Mesoporous Mater.*, 2019, **288**, 109603.
29 M. Åhlén, A. Jaworski, M. Strømme and O. Cheung, *Chem. Eng. J.*, 2021, **422**, 130117.
30 W.-L. Xue, P. Kolodzeiski, H. Aucharova, S. Vasa, A. Koutsianos, R. Pallach, J. Song, L. Frentzel-Beyme, R. Linser and S. Henke, *Nat. Commun.*, 2024, **15**, 4420.
31 Y. Pan, D. Heryadi, F. Zhou, L. Zhao, G. Lestari, H. Su and Z. Lai, *CrystEngComm*, 2011, **13**, 6937–6940.
32 J. A. Boissonnault, A. G. Wong-Foy and A. J. Matzger, *J. Am. Chem. Soc.*, 2017, **139**, 14841–14844.
33 R. Ahmad, U. A. Khan, N. Iqbal and T. Noor, *RSC Adv.*, 2020, **10**, 43733–43750.
34 Y. Wang, Y. Wang, L. Zhang, C.-S. Liu and H. Pang, *Inorg. Chem. Front.*, 2019, **6**, 2514–2520.
35 E. P. Valadez Sánchez, H. Gliemann, K. Haas-Santo, C. Wöll and R. Dittmeyer, *Chem. Ing. Tech.*, 2016, **88**, 1798–1805.
36 S. Panda, S. Kundu, P. Malik and R. Haldar, *Chem. Sci.*, 2024, **15**, 2586–2592.
37 M. Ahmad, R. Patel, D. T. Lee, P. Corkery, A. Kraetz, Prerna, S. A. Tenney, D. Nykypanchuk, X. Tong, J. I. Siepmann, M. Tsapatsis and J. A. Boscoboinik, *ACS Appl. Mater. Interfaces*, 2024, **16**, 27887–27897.
38 P. Malik and R. Haldar, *Mol. Syst. Des. Eng.*, 2022, **7**, 873–877.
39 S. Panda, T. Maity, S. Sarkar, A. K. Manna, J. Mondal and R. Haldar, *Nat. Commun.*, 2025, **16**, 1231.
40 K. Zhang, R. P. Lively, M. E. Dose, A. J. Brown, C. Zhang, J. Chung, S. Nair, W. J. Koros and R. R. Chance, *Chem. Commun.*, 2013, **49**, 3245–3247.
41 O. Zybaylo, O. Shekhah, H. Wang, M. Tafipolsky, R. Schmid, D. Johannsmann and C. Wöll, *Phys. Chem. Chem. Phys.*, 2010, **12**, 8093–8098.
42 S. Kundu, T. Maity, S. Panda and R. Haldar, *Chem.–Eur. J.*, 2024, **30**, e202403607.